JOURNAL OF PROPULSION AND POWER
Vol. 11, No. 6, November–December 1995

Structure of a Swirl-Stabilized Combusting Spray

Daniel L. Bulzan*
NASA Lewis Research Center, Cleveland, Ohio 44135

Measurements of the structure of a swirl-stabilized, reacting spray are presented. The configuration consisted of a research air-assist atomizer located in the center surrounded by a coflowing airstream. Both the air-assist and coflow streams had swirl imparted to them in the same direction with 45-deg angle swirlers. The fuel and air entered the combustor at ambient temperature and the combustor was operated in an unconfined environment. The gas phase was seeded with aluminum–oxide particles in order to obtain velocity measurements. Mean velocity measurements for the gas phase are reported for both an isothermal, single-phase case without drops and a reacting spray case at axial distances from 2.5 to 50 mm downstream of the nozzle. Heptane fuel was used for all the experiments. Drop size and mean velocity and drop number flux are also reported for five axial distances downstream. The measurements were performed using a two-component phase/Doppler particle analyzer. Profiles across the entire flowfield where velocities were significant are presented. Mean gas-phase temperatures were also measured intrusively using a single pt/pt-13%rh thermocouple and are also reported at axial distances from 2.5 to 50 mm downstream of the nozzle.

Introduction

COMBUSTING sprays are very important for a large number of propulsion applications. Important physical processes involved in combusting sprays are the interactions between the droplets and the gas phase, the vaporization of the droplets, and chemical reaction with associated heat release. These physical processes are all coupled and can only be completely described using numerical modeling. As part of an effort to improve the numerical modeling of spray combustion for gas-turbine combustors, an experimental study has been performed to obtain a data set for a liquid-fueled combustor with simplified geometry that can be used for comparison with numerical models.

Because of their numerous practical applications, swirling flows with combustion have been studied by a large number of investigators. Earlier reviews of swirling flows both with and without combustion are presented by Chigier,[1] Syred and Beer,[2] and Lilly.[3] These papers predate the development of nonintrusive, laser-based diagnostics; consequently, all of the results described were obtained using intrusive instrumentation and detailed structure measurements for these types of flows were not possible.

With the advent of newer instrumentation techniques, namely laser Doppler anemometry (LDA), velocity measurements could be obtained and additional details of the structure of these types of flows began to emerge. LDA velocity measurements in spray flames are reported by Styles and Chigier[4] and Khalil and Whitelaw.[5] They reveal some of the flowfield structure of swirling flames, but drop size and size-correlated velocity measurements were not possible.

The development of the phase/Doppler particle analyzer,[6] enabled the simultaneous measurement of droplet size and velocity. This instrument has been used by a number of investigators for measurements in spray flames in a variety of configurations. Mao et al.[7] present phase/Doppler measurements of Sauter mean diameter (SMD), mean axial drop velocity, drop number density, and liquid flux in a swirl-stabilized unconfined spray flame using an air-assist atomizer. No gas-phase results are reported and the measurements were taken from 10 to 75 mm downstream of the nozzle. McDonell and Samuelsen[8] present measurements taken using a two-component phase/Doppler system in a model can combustor under reacting and nonreacting conditions. The measurements were reported from 50 to 100 mm downstream of the nozzle. Edwards et al.[9] report drop size, drop velocity, drop size distribution, and liquid volume flux in a swirl-stabilized, semiconfined flame at 10–100 mm downstream of the nozzle. Gas-phase velocities are reported at axial locations from 25 to 100 mm downstream using a combination of standard LDA with gas-phase seeding and phase/Doppler measurements for 2-μm drops where possible. No gas-phase results are reported at 10 mm downstream. Edwards and Rudoff[10] report mean drop and gas-phase velocity vectors for the same configuration. The gas-phase measurements were obtained using a standard LDA system with seeding particles and were reported to be "biased" in regions where a substantial number of drops were present. Ghaffarpour and Chehroudi[11] present phase/Doppler measurements in a swirl-stabilized, confined combustor at axial locations from 15 to 100 mm downstream of the nozzle. Mean drop velocities and SMD are reported at six axial locations. Gas-phase velocity was measured using LDA without drops or combustion. Phase/Doppler measurements of drop size and velocity as well as gas-phase velocity in a swirl-stabilized combusting spray are reported by McDonell and Samuelsen.[12] The combustion airflow was seeded in order to make the gas-phase measurements. Measurements are reported at axial distances of 50, 75, and 100 mm downstream of the nozzle. Hassa et al.[13] present phase/Doppler measurements in a cylindrical combustor using an air-assist atomizer at axial distances from 7 to 97 mm downstream of the nozzle. Both drop and gas-phase velocities are reported. Gas-phase measurements in the reacting flowfield were made using the smaller drops as tracing particles. This required some judgement in order to determine what size drops should be used to represent the gas phase and also required the use of larger drops to represent the gas phase at larger axial distances due to an absence of smaller drops. Temperature measurements were also provided. McDonell et al.[14] present extensive phase/Doppler measurements of drop size and velocity, gas-phase velocity, temperature, and methanol gas concentration for an air-assist atomizer. Measurements are reported from 7.5 to 100 mm downstream of the nozzle and are pro-

Received May 7, 1994; revision received Jan. 3, 1995; accepted for publication Jan. 30, 1995.

*Aerospace Engineer, Aerothermochemistry Branch, M/S 5-11.

vided for single-phase, nonreacting spray, and reacting spray cases. The spray was injected downward for all test conditions and only the air-assist stream was utilized to stabilize the flame.

Measurements of drop size are also available using other techniques. Presser et al.[15] reported drop SMD measurements in a swirl-stabilized confined flame from 10 to 76 mm downstream of the nozzle using an ensemble light-scattering technique. Mean drop velocity measurements were obtained using standard LDA. Gas-phase measurements are reported only for the combustion air under isothermal conditions without the presence of the drops. A comparison of drop sizes measured using three techniques is reported by Zurlo et al.[16] Measurements were obtained using the ensemble scattering/polarization ratio, phase/Doppler and light intensity deconvolution techniques. Mean drop size and number–density measurements were not the same due to the selective sensitivity of each technique to a different size range.

These measurements in swirl-stabilized spray flames have been very useful in providing detailed information regarding the structure of these flowfields. Some of the data from them are also useful for the development of computer models. Most, however, do not provide enough detailed information for both the liquid and gas phases for the development of models, especially for initial conditions close to the nozzle. Hassa et al.[13] provide the nearest measurements at 7 mm from the nozzle, and McDonell et al.[14] provide measurements at 7.5 mm downstream. In the present study data are presented at locations as close as 2.5 mm from the nozzle in order to provide better initial conditions and also study the two-phase flow near the injector. The same nozzle is used for the present study as that reported in Ref. 14, however, a coflowing stream with swirl is also utilized in the present study in order to simulate conditions that are more representative of those found in a gas-turbine combustor.

Experiment

Apparatus

The present study is an attempt to provide a set of measurements that can be used in order to gain a better understanding of the physics for swirl-stabilized spray flames. The combustor utilized in the present experiment is illustrated in Fig. 1. It consists of a center-mounted air-assist fuel nozzle, Parker Hannifin research simplex air-assist atomizer, surrounded by a coflowing airstream. The nozzle orifice diameter was 4.8 mm. Both the air-assist and the coflow airstreams had swirl imparted to them using 45-deg swirlers. The swirlers were constructed by machining 45-deg slots into rings. Both streams were swirled in the same direction for the present study. The combustion air was not preheated and entered the combustor at 297 ± 3 K. The top of the air-assist nozzle was water cooled to prevent overheating of an o-ring in the nozzle assembly and maintain the atomizing air and liquid fuel at a constant inlet temperature of 297 ± 3 K. The temperatures of the fuel, atomizing air, and coflow airstreams were measured using Chromel Alumel thermocouples. Flow rates of the airstreams were measured using calibrated orifices and the fuel flow rate was measured using a mass flow meter. A single set of operating conditions was chosen where the combustor operated in a stable mode, soot was relatively minor, and measurements could be taken near the injector itself. All results reported in the present study were taken at a coflow airflow rate of 13.1 g/s, an air-assist flow rate of 0.96 g/s, and a fuel flow rate of 0.30 g/s. Uncertainty in these flow rates is estimated at ±5%. At these flow conditions the pressure drop through the nozzle was 23.4 kPa for the fuel and 19.3 kPa for the atomizing air. The atomizing air pressure drop through the nozzle remained constant for both the liquid-fueled and single-phase cases. The fuel used was heptane. The coflow stream entered the combustor at three radial locations, passed through a honeycomb flow straightener, and then the swirler before exiting the combustor. The swirler was located 140 mm upstream of the combustor exit in order to minimize wakes from the swirler. The flow from the combustor discharged upwards into ambient, stagnant surroundings. A photograph of the combustor in operation is shown in Fig. 2. A laser light sheet with a thickness of approximately 1 mm was passed through the center of the flowfield and used to illuminate the droplet stream. The photograph was taken at 90 deg relative to the laser light sheet. It is evident that a few very large drops are able to penetrate the combustion zone with a relatively straight trajectory. Based upon a number of such photographs, the bright blue region near the nozzle appeared very steady while the yellow luminous soot region showed some variation with time. The combustor was mounted vertically within a large (1.8 m square by 2.4 m high) enclosure. The top of the nozzle was located 1.1 m from the floor of the enclosure and 1.4 m below the screened inlet of the exhaust hood at the 2.5-mm axial measurement location. The entire enclosure was mounted on two sets of linear bearings and was traversed using stepper motors to provide motion in two directions. The combustor assembly itself could be traversed in the vertical direction using a third stepper motor to allow measurements at all locations in the flowfield. This arrangement allowed rigid mounting of all optical components.

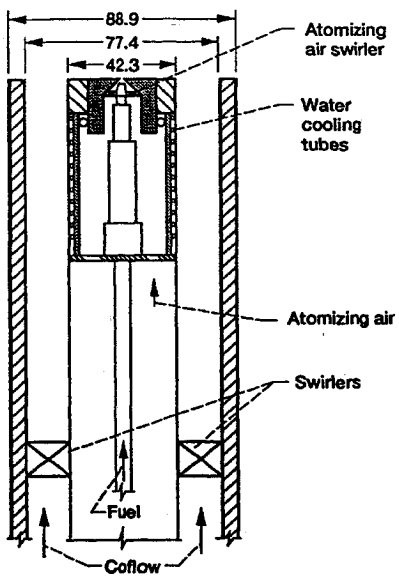

Fig. 1 Schematic drawing of the combustor.

Fig. 2 Photograph of swirl-stabilized, spray flame.

Instrumentation

A phase/Doppler particle analyzer was used for all velocity and size measurements. A two-component system using green (514.5-nm) and blue (488.0-nm) beams from an argon–ion laser operating at 1.5 W power output was used for the measurements. The transmitting optics utilized a 500-mm focal length lens combined with a 300-mm focal length collimating lens to yield a focused beam waist of 131 μm for the green and 124 μm for the blue lines. The fringe spacing was 6.788 μm for the green and 6.667 μm for the blue lines. The receiving optics were located 30 deg off-axis in the forward-scatter direction. Light was collected using a 500-mm focal-length f 5.4 lens and then focused onto a 100 μm by a 1 mm long slit. Details of the instrument can be found in Ref. 6.

In the present study, velocities of both the liquid and gaseous phases were measured. This was accomplished by seeding the gas phase with nominal 1-μm aluminum–oxide particles. The coflow, air-assist flow, and the ambient surroundings were all seeded to minimize biasing due to concentration gradients. Phase discrimination is inherent in the instrument with the ability to size each measured particle. At each spatial location, two measurements were taken in order to measure the velocity of each phase. A threshold voltage for the photodetectors at the specified laser power was determined experimentally, below which signals from the aluminum–oxide particles were not detected. For the drop measurements, the photodetector voltage was kept below this threshold value in order to eliminate interference from the aluminum–oxide particles. This threshold voltage was typically about 125 V above that required for the drop measurements; therefore, this technique did not eliminate smaller drops and drops in the 1-μm range were recorded using this approach. Particles with diameters smaller than 2.4 μm were used to represent the gas-phase velocity. Two complete traverses at each axial station were performed in order to measure all three components of velocity and provide a check on flow symmetry. Each traverse measured axial velocity and either radial or tangential velocity. Comparing the two orthogonal traverses gave essentially identical values of axial velocity, drop size, and number flux within the stated accuracy of the measurements. Generally, 64,000 measurement attempts were made at each measurement location. In regions where there were few drops, data was taken for a minimum of 600 s. The percentage of validated measurements varied depending on the number density, size distribution, and velocities of drops at each location, but generally ranged from about 65 to 90% for the drop measurements. Validation with particle sizing for the gas-phase measurements using the aluminum–oxide seeding particles was much lower and generally averaged about 20%. Where drops were not present in the flowfield, the gas-phase measurements of velocity were taken with sizing disabled. Tests at these locations showed essentially no difference in measured values with the sizing disabled compared to measurements taken with the sizing enabled.

Gas-phase mean temperatures were measured using a single pt/pt-13%rh thermocouple traversed through the flowfield. The 16-cm-long thermocouple had a metal sheath 1.59 mm in diameter for rigidity. It was insulated with high-temperature alumina and had an exposed junction with a bead diameter of 0.5 mm. Thermocouple voltages were sampled at a rate of 1250 Hz using a 12-bit analog to digital signal conversion board. The reference temperature was taken at the terminal strip where voltages were measured and updated with each measurement. Each temperature measurement reported represents a time-averaged reading for 5 s. No attempt was made to shield the junction from drop impingement since the flowfield was noticeably disturbed when the thermocouple was introduced directly into the spray region. This is reflected in the results where immersion in the spray produced very low temperatures. Values in these regions should not be considered quantitative for gas-phase temperatures. At locations outside of the spray region, the presence of the thermocouple did not have a noticeable effect on the flame.

Uncertainty Analysis

Uncertainty in position measurements is estimated to be ± 0.2 mm for both radial and axial measurements. Uncertainty in velocity and temperature measurements was estimated by measurement repetition at a number of points in the flowfield. Drop size uncertainty in an isothermal monodisperse drop stream is estimated at $\pm 6.5\%$ based on calibration and probably is larger in an evaporating spray containing a size distribution. Since the liquid drop temperature in the flowfield could not be measured, a constant index of refraction for heptane at 298 K was used for all reported measurements. The refractive index is estimated to decrease by about 5% from 298 K to the boiling temperature of heptane, 371 K. Tests with a monodisperse drop generator indicated that this change in refractive index decreases the measured drop size by 7%; therefore, this is the maximum size error due to the variation in refractive index. For drop velocities, uncertainty is estimated at $\pm 10\%$. Since the gas-phase measurements require sizing of a very small particle where drops are present, the uncertainty is larger than the drop velocity and is estimated at $\pm 18\%$. Uncertainty in gas-phase mean velocity where mean velocity is very small and turbulence is relatively large is higher and is estimated to be $\pm 50\%$. These conditions are found near the centerline for radial and tangential velocities and in the entrainment region at the outer edge of the flowfield for all three velocity components. Uncertainties in uncorrected temperature measurements are estimated to be $\pm 10\%$. Drop number–flux measurement is the most difficult measurement to make because it requires an accurate measurement of drop size, velocity, and probe volume size. This measurement is quite difficult in the present flowfield where there are three substantial velocity components. This is complicated by the fact that the laser-beam power distribution is Gaussian and probe volume size is a function of drop size. In addition, in dense regions of the spray, more than one drop can be present in the probe volume at one time causing rejection of the signal, which leads to an underestimation of the volume flux of the liquid phase. In the present set of measurements, integrating the liquid-flux measurements across the flowfield gave 26.6% of the metered flow rate at 2.5 and 27.0% at 5, 47.8% at 10, 23.0% at 20, and 2.6% at 50 mm downstream of the nozzle. Since the largest volume flux should be measured at 2.5 mm downstream, the measurements reported for drop number flux at 2.5 and 5 mm downstream are certainly lower than they should be due to the high number densities at these axial locations. In order to use the data for validation it is recommended that the measured number fluxes be increased at the initial measurement location to give the measured fuel flow rate.

Results and Discussion

Gas Phase

Results are presented for axial locations of 2.5, 5, 10, 20, and 50 mm downstream of the nozzle. Gas-phase mean axial velocities are presented in Fig. 3 for isothermal, single-phase flow without drops and two-phase flow with combustion at these axial locations downstream of the nozzle. The symmetry of the flowfield is readily apparent. The two 45-deg angle swirlers induce a central recirculation zone along the axis of the flowfield. At 2.5 mm downstream, the reacting two-phase flow and the isothermal single-phase flow show similar results for mean axial velocity. At this axial location, the maximum mean axial velocity for the reacting case is slightly larger and its radial location is shifted slightly outward compared to the isothermal case. The recirculation zone extends upstream of the first measurement station. This is illustrated by the data at 2.5 mm downstream, where there is a small region in the

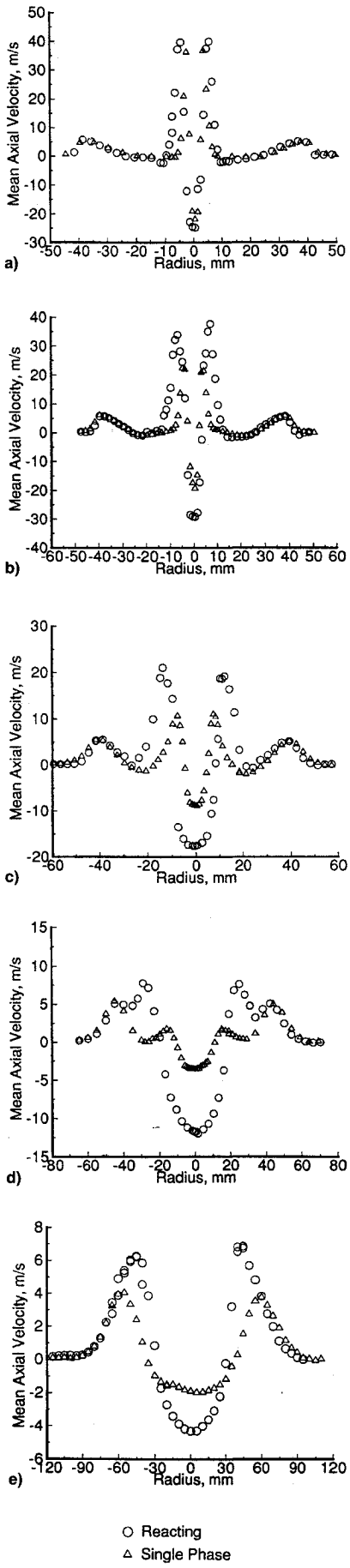

Fig. 3 Gas-phase mean axial velocity profiles: a) 2.5, b) 5, c) 10, d) 20, and e) 50 mm downstream.

center where negative velocities are present. Centerline measurements were attempted at locations closer to the nozzle and indicated that the negative velocities at the centerline persist until approximately 1 mm from the nozzle. The two peaks in axial velocity are due to the air-assist stream issuing from the center orifice of the nozzle and the coflow stream. The very low axial velocities at radii between 10–20 mm are caused by the top of the nozzle between the central orifice and the coflow airstream. At 5 mm downstream there are larger differences in axial velocity between the reacting and single-phase cases. The maximum axial velocity and radial location of the peak velocity have increased for the reacting case due to gas expansion caused by the heat release. Beyond a radius of about 15 mm, no differences are apparent between the reacting and single-phase cases. The negative velocities in the recirculation zone have increased for the reacting case and decreased for the single-phase case compared to the results obtained at 2.5 mm downstream. Similar trends are illustrated at 10 and 20 mm downstream of the nozzle. At 20 mm downstream, the maximum axial velocity in the flowfield originating from the coflow stream is larger than that from the air-assist stream for the single-phase case. This is reversed for the reacting case. At 50 mm downstream, the air-assist and coflow streams have merged and only one axial velocity peak is evident. For the reacting case, the maximum velocity increases, and the radial location of the maximum velocity decreases compared to the single-phase case. At 200 mm downstream, the reacting case has a positive axial velocity at the center indicating the recirculation zone has closed, however, the single-phase case still has a slight negative axial centerline velocity at this axial location. Measurements were obtained at axial distances as far downstream as 350 mm from the nozzle.

Mean radial velocities for the gas phase are presented in Fig. 4 for the same axial locations downstream of the nozzle. Even at the initial measurement location of 2.5 mm downstream, large differences are apparent in radial velocity between the reacting and single-phase cases. Maximum radial velocity has increased to about 45 m/s for the reacting case compared to 15 m/s for the single-phase case due to heat release and expansion of the gas. The increased recirculation zone strength for the reacting case causes the gas to expand more rapidly in the radial direction than the axial direction. The radial location for the maximum velocity has also increased for the reacting case compared to the single-phase case. Mean radial velocities at radii larger than about 15 mm are essentially identical for the single-phase and reacting cases at 2.5 mm downstream. At 5, 10, and 20 mm downstream, peak mean radial velocities and radial locations for the peak velocity are considerably increased for the reacting case compared to the single-phase case. Negative radial velocities in the recirculation zone are also increased for the reacting case compared to the single-phase case. At axial distances of 50 mm and greater, peak positive radial velocities are similar for the two cases.

Mean tangential velocities for the gas phase are presented in Fig. 5 for the same axial locations downstream of the nozzle. At axial distances of 2.5–10 mm downstream, peak tangential velocities from the air-assist stream are reduced for the reacting case compared to the single-phase case. Due to the expansion of the gas and the presence of the drops, a decrease is observed in the mean gas-phase angular velocity for the reacting case compared to the single-phase case. Similar to the results shown for the axial and radial velocities, the radial location for the peak mean tangential velocity is also shifted outward for the reacting case. No differences are apparent between the reacting and single-phase cases for the outer mean tangential velocity peak from the coflow stream at axial distances of 10 mm and less. At axial distances of 20 mm and larger, the situation is reversed and the reacting case has larger mean tangential velocities compared to the single-phase case.

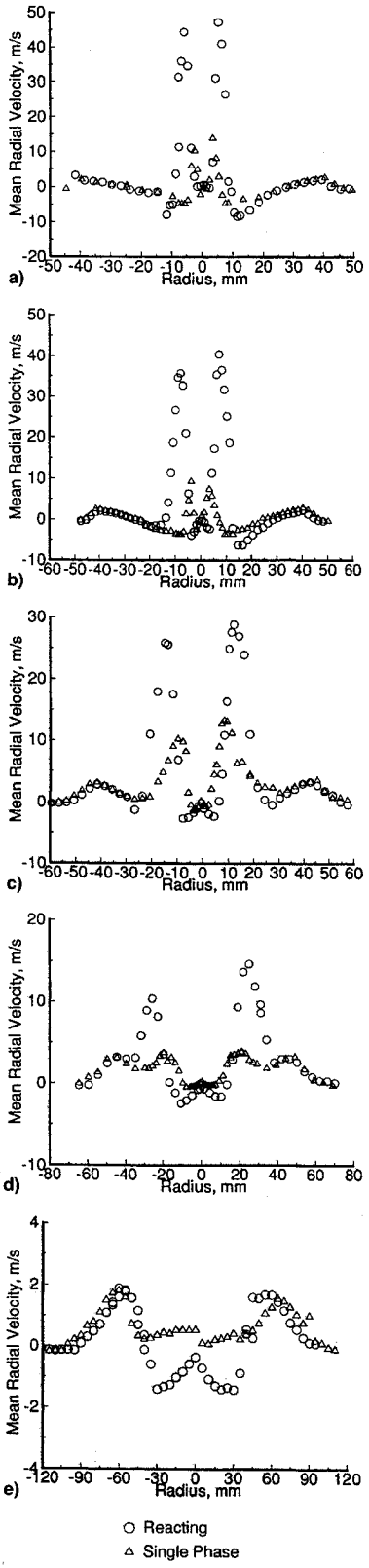

Fig. 4 Gas-phase mean radial velocity profiles: a) 2.5, b) 5, c) 10, d) 20, and e) 50 mm downstream.

Two distinct peaks are evident at axial distances of 20 mm and less. The peak nearest the center is due to the swirler in the air-assist stream and the outer peak is caused by the swirler in the coflow airstream. At axial distances of 50 mm and larger, the air-assist and coflow streams have merged to give a single tangential velocity peak, similar to the results shown for axial velocity.

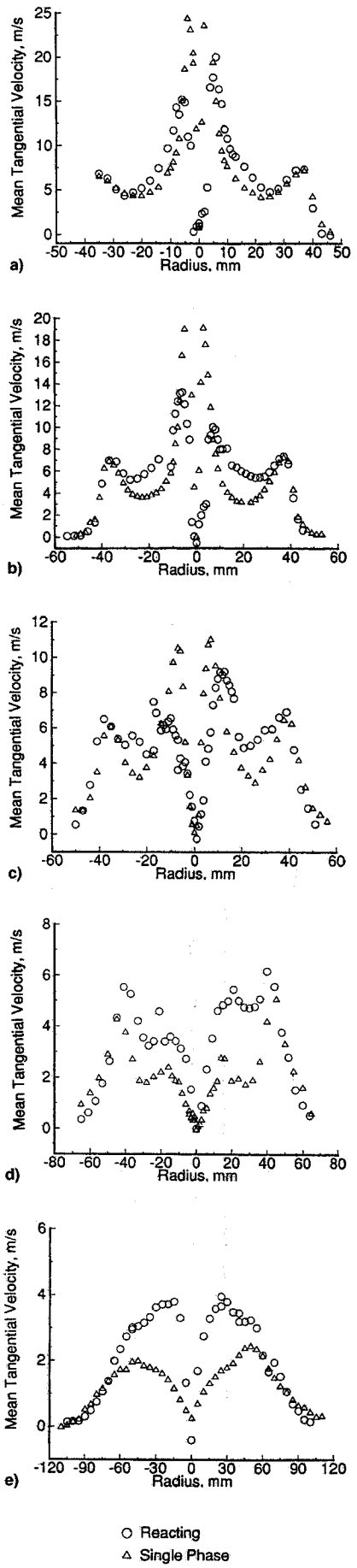

Fig. 5 Gas-phase mean tangential velocity profiles: a) 2.5, b) 5, c) 10, d) 20, and e) 50 mm downstream.

Liquid Phase

The mean axial velocity for the drops is illustrated in Fig. 6. Results are presented at downstream locations of 2.5, 5, 10, 20, and 50 mm downstream of the nozzle. As discussed in Ref. 14, this atomizer is described as a "prompt" atomization nozzle due to the strong jet of air blasting the liquid jet. Images obtained in the present investigation using a short duration (less than 10 ns) laser-light pulse confirmed that no ligaments were present at 2.5 mm downstream. At a measurement position of 100 mm downstream, not enough drops were present to have confidence in the velocity measurements. Results are illustrated for drop diameters of 6.9, 15.4, 23.8, 40.8, 66.2, and 97.2 μm. Each drop diameter has a size range of 2.8 μm. Velocity measurements for a particular size are not presented at locations where not enough valid measurements were obtained. This is particularly true for the larger drop sizes. This was determined by examining the size–velocity correlation to determine whether the measured velocity was reasonable. The specific cutoff point was generally found to be about 30 samples. Gas-phase measurements for the combusting case are illustrated by a solid line representing a spline-fit between the measured data points. At axial locations of 2.5 and 5 mm downstream, it is evident that the smaller drops follow the gas-phase velocity more closely than larger drops. In the recirculation zone, even the 6.9-μm drops lag the gas phase by a considerable amount. This was also observed by Hassa et al.[13] At 2.5 mm downstream, the drops are only found in a narrow region of the flow. A relatively large velocity difference between various drop sizes is also apparent. This is especially evident at 5 mm downstream, where the peak axial velocity of the 66-μm drops is about 20 m/s lower than the velocity of the 6.9-μm drops. In the recirculation zone at 5 mm downstream, only drops with diameters of 23.8 μm and smaller have negative axial velocities. The larger drops have enough momentum to retain positive values of axial velocity in the recirculation zone at this axial location. At 10 mm downstream, the axial velocity is changing very rapidly as the air-assist stream containing the drops encounters the negative velocities in the recirculation zone. The result is that the peak mean axial velocity for the 40.8-μm drops is similar to the gas phase. The peak velocities of the 6.9- and 15.4-μm drops are nearly identical as the drop velocities adjust to the rapidly changing gas phase flowfield. It is also important to realize that drop size is continually decreasing in this flowfield and a 6.9-μm drop at 10 mm downstream was a larger drop upstream of this measurement location. This effect causes an increase in the slip velocity between the gas and the drops throughout the flowfield. At 20 mm downstream, the radial location of the peak velocities of the drops coincides with the edge of the recirculation zone. The drop velocities continue to adjust to this rapidly changing gas phase. This is illustrated by the more rapid decrease in the velocity of the 6.9-μm drops compared to larger drops. The adjustment in drop velocity is complete by 50 mm downstream where it is evident that the smallest drops again show the least amount of slip with the gas phase. At 50 mm downstream, the drops have larger velocities than the gas phase and the larger drops generally have higher velocities, except for the 66.2-μm drops. At axial distances of 10 mm downstream and larger, essentially no drops are found in the central regions of the flowfield. Due to the evaporation of the drops, very few larger drops are found at 50 mm downstream of the nozzle.

Measurements of mean radial velocity for the drops are presented in Fig. 7 for the six drop diameters at the same five axial distances downstream of the nozzle. Again, the gas-phase measurements are indicated by a solid line. Results for mean radial velocity are very similar to those previously observed for axial velocity. At axial distances of 2.5 and 5 mm downstream, the size–velocity correlation is very ordered with the 6.9-μm drops tracking the gas-phase flowfield more closely

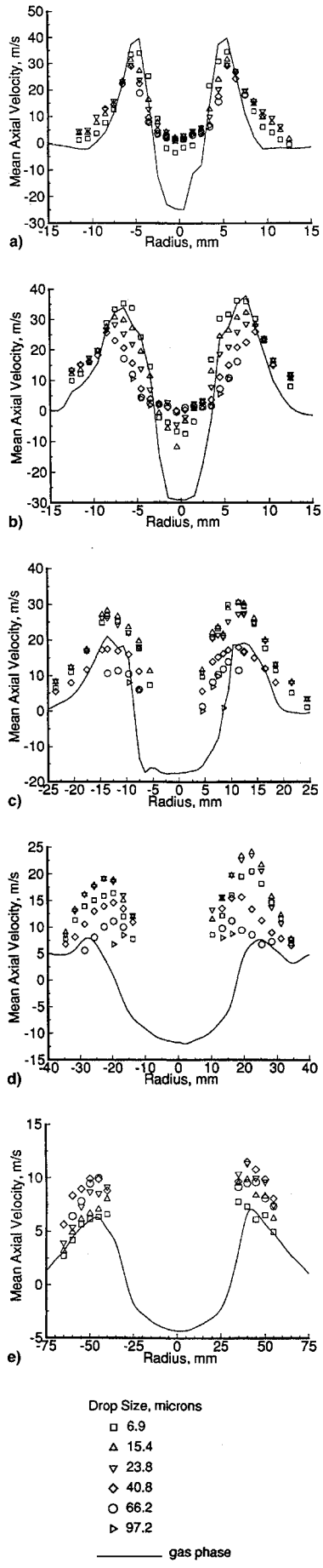

Fig. 6 Drop mean axial velocity profiles: a) 2.5, b) 5, c) 10, d) 20, and e) 50 mm downstream.

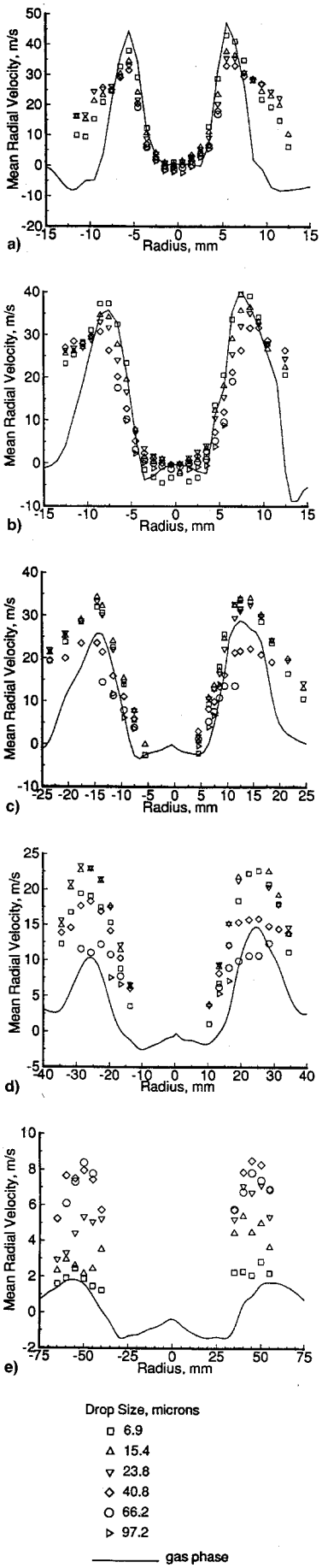

Fig. 7 Drop mean radial velocity profiles: a) 2.5, b) 5, c) 10, d) 20, and e) 50 mm downstream.

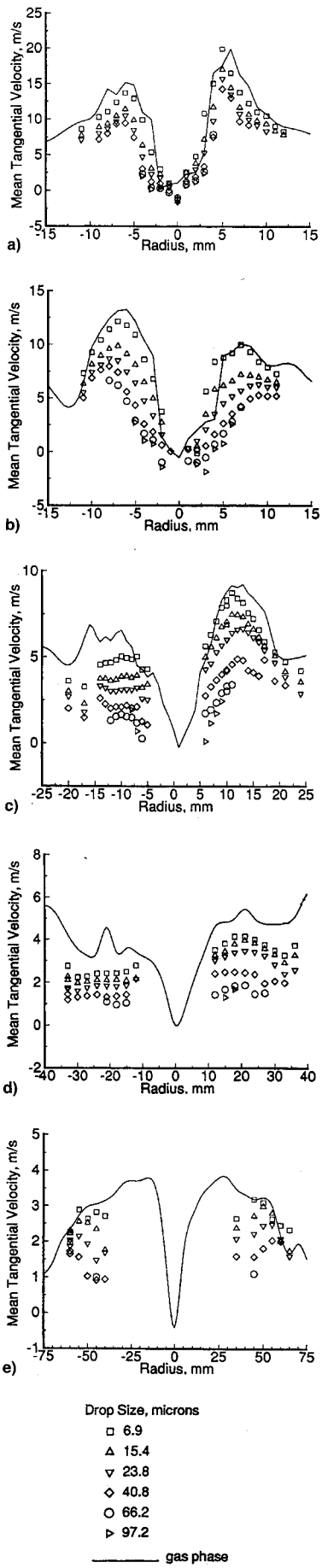

Fig. 8 Drop mean tangential velocity profiles: a) 2.5, b) 5, c) 10, d) 20, and e) 50 mm downstream.

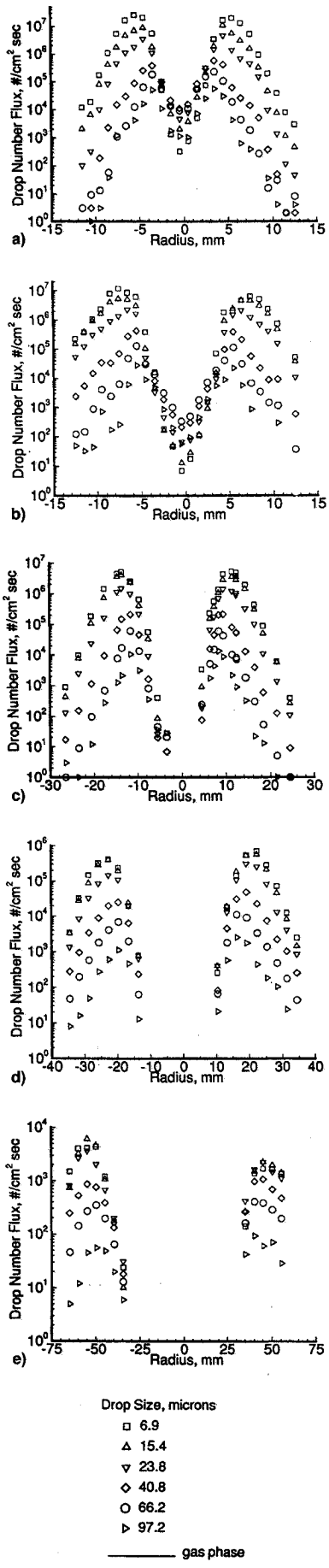

Fig. 9 Drop number–flux profiles: a) 2.5, b) 5, c) 10, d) 20, and e) 50 mm downstream.

than the larger drops. At the outer edge of the flowfield, the gas-phase radial velocity decays quite rapidly resulting in relatively large slip velocities between the drops and the gas phase, even for the 6.9-μm drops. At 5 mm downstream, only the smaller drops are carried into the recirculation zone, illustrated by their negative radial velocities. At 10 and 20 mm downstream, as previously discussed for axial velocity, the gas-phase mean radial velocity is also changing very rapidly as the air-assist stream is strongly influenced by the central recirculation zone. The momentum of the evaporating drops present at these axial locations causes their velocities to be significantly different than the gas phase. At 50 mm downstream, the drop velocities have adjusted to the gas-phase flowfield and the smaller drops again show the least amount of slip with the gas phase. Similar to the results previously shown for axial velocity, the larger drops have significantly larger velocities than the gas phase at this distance downstream.

Mean tangential velocity measurements for the drops are presented in Fig. 8 for the same six drop sizes and axial locations as the previous two figures. It is apparent that the tangential velocities are considerably lower and not as symmetric as previously observed for axial or radial velocities. At all axial locations, the size–velocity correlation is very uniform for mean tangential velocity. The larger drops have lower mean tangential velocities than smaller drops. The gas-phase tangential velocity does not undergo the very rapid changes observed for the radial and axial velocities and the drops are able to adjust to the changes. Again, very few large drops are found at the 50-mm downstream location due to the evaporation of the drops.

Drop number fluxes for the six drop sizes are presented in Fig. 9. The results are provided as the number of drops/(cm^2 s) and are plotted on a log scale. The instrument divides the drop size distribution into 50 size bins. These 50 bins were combined into 10 sizes in order to make the data set manageable. In this figure, 6 of the 10 combined drop size bins are presented. The diameters presented represent mean values of size bins with a width of 8.5 μm for the 6.9-, 15.4-, 23.8-, and 40.8-μm drops, a width of 14.2 μm for the 66.2-μm drops, and a width of 19.2 μm for the 97.2-μm drops. To adequately account for all the measured drops, the number fluxes for the remaining four sizes would also be required. The nozzle used in the present study produced a very large number of relatively small drops, evident in the results at 2.5 mm downstream. Number flux increases with decreasing drop size, reaching a maximum at a radius of about 6 mm at 2.5 mm downstream. The maximum number fluxes show a variation of four orders of magnitude between the large and small drop sizes. Drop number fluxes decrease slightly between 2.5, 5, and 10 mm downstream. As previously discussed, integrated volume fluxes increased between 2.5–10 mm downstream even though actual number-flux values decrease, because the drops are found at larger radii. Between 10–20 mm downstream, number fluxes substantially decrease as does the integrated volume flux. At 50 mm downstream, most of the drops have evaporated and the remaining drops are smaller. Very few drops are found in the center at 2.5 mm downstream and by 10 mm downstream of the nozzle essentially no drops are found in the central recirculation zone. There is a slight asymmetry evident in the number fluxes at 5 and 50 mm downstream. The positive values of radius have slightly reduced number fluxes compared to the negative side. Integrated liquid volume fluxes generally were also larger for the negative side.

Temperature

Gas-phase average temperatures are presented in Fig. 10. Radial profiles are presented for axial locations from 2.5 to 50 mm downstream of the nozzle. Results are presented illustrating both the temperature measurements as taken and

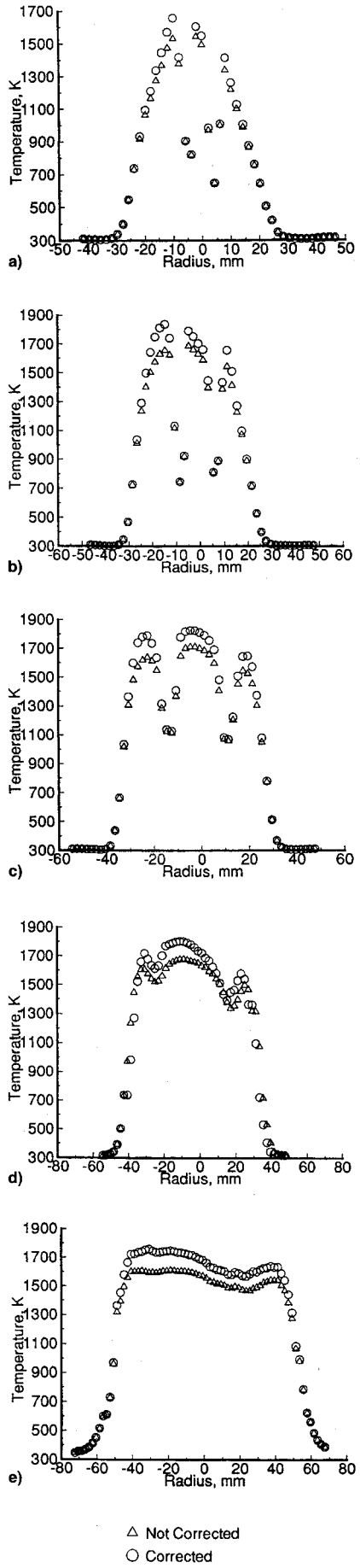

Fig. 10 Gas-phase temperature profiles: a) 2.5, b) 5, c) 10, d) 20, and e) 50 mm downstream.

the measurement corrected for radiation heat loss from the thermocouple. The radiation correction was performed similar to Shuen et al.,[17] considering only radiation heat loss to ambient surroundings and neglecting any radiation heat transfer from the soot present in the flame. The temperature corrections varied with temperature level up to a maximum of about 150 K. At 2.5 mm downstream, gas-phase temperature is substantially elevated over the inlet temperature and has a maximum corrected temperature of about 1650 K. The dramatic reductions in temperature for 2.5 mm downstream at a radius of about 5 mm are caused by droplet impingement on the thermocouple bead; therefore, these measurements are not realistic gas-phase temperatures. No attempt was made to shield the thermocouple from the drops because the presence of even the small thermocouple bead in the spray caused visible distortion in the flowfield. A nonintrusive technique is required for accurate gas-phase temperature measurements in regions where substantial numbers of drops are present. At 5 mm downstream, maximum temperatures have increased to about 1840 K. The sharp reductions in temperature due to droplet impingement are still present and are found at a radius of about 9 mm. At 10 mm downstream, the maximum corrected temperature is about 1825 K and the width of the higher temperature region is larger. Drop impingement is still evident at a radius of about 15 mm. At 20 mm downstream, the drop number density has substantially decreased (see Fig. 9), and this is reflected in smaller temperature reductions due to drop impingement at a radius of about 21 mm. Similar trends are evident at axial locations farther downstream. Some asymmetry is evident in the temperature profiles, with the negative radius having a higher temperature than the positive. This side had generally higher measurements of volume flux indicating an increase in fuel–air ratio for the negative side compared to the positive.

Conclusions

Gas-phase axial velocity is increased for the combusting spray case compared to the single-phase isothermal case due to the gas expansion caused by the heat release. The strength of the recirculation zone is also increased for the reacting case and the overall length of the recirculation zone is shorter compared to the single-phase case. At axial distances up to 20 mm downstream of the nozzle, gas-phase mean radial velocities are substantially increased for the reacting spray compared to the single-phase case. Gas-phase tangential velocities are reduced for the reacting spray case compared to the single-phase case due to the presence of the drops and the gas expansion due to heat release. At 2.5 mm downstream, negative axial velocities were measured for a small region at the center of the flowfield for both the reacting and single-phase cases.

Mean axial and radial velocities for the drops lag the gas-phase velocities at axial distances of 2.5 and 5 mm downstream. At these axial distances downstream, the slip velocity increases with increasing drop size. At 10 and 20 mm downstream, the drop axial and radial velocities are adjusting to the rapidly changing gas-phase flowfield and the velocity correlation with drop size is not as uniform as observed at smaller distances downstream. At 50 mm downstream, mean drop axial and radial velocities are larger than the gas phase.

Mean tangential velocities for the drops lag the gas phase at all axial locations downstream of the nozzle. A size–velocity correlation is very apparent with the smaller drops showing the least amount of slip with the gas phase. At 20 mm downstream, the largest velocity difference between the gas phase and the drops is observed.

Drop number fluxes at 2.5 mm downstream illustrate the drop size distribution produced by the research air-assist atomizer used in the present study. Number fluxes were directly related to drop size with smaller sizes having larger numbers of drops. Drop number fluxes decreased slightly between 2.5–

5 mm downstream and then steadily decreased. At 50 mm downstream drop number fluxes are considerably reduced as well as the number of larger drops.

Mean gas-phase temperatures show elevated temperatures at the first axial measurement location of 2.5 mm downstream of the nozzle due to a small region with negative axial velocities. Maximum gas-phase temperatures were observed at 5 mm downstream of the nozzle and then decreased as axial distance increased. Drop impingement on the thermocouple bead produced very low temperatures in regions where the number of drops were substantial.

Acknowledgments

The author would like to acknowledge the assistance of Sylvia Merritt in the processing of the phase/Doppler data and Viviannette Sánchez in the acquisition and processing of the gas-phase temperature data.

References

[1]Chigier, N. A., "Gas Dynamics of Swirling Flow in Combustion Systems," *Astronautica Acta*, Vol. 17, Nos. 4–5, 1972, pp. 387–395.

[2]Syred, N., and Beer, J., "Combustion in Swirling Flows: A Review," *Combustion and Flame*, Vol. 23, Aug.–Dec., 1974, pp. 143–201.

[3]Lilley, D. G., "Swirl Flows in Combustion: A Review," *AIAA Journal*, Vol. 15, No. 8, 1977, pp. 1063–1078.

[4]Styles, A. C., and Chigier, N. A., "Combustion of Air Blast Atomized Spray Flames," *Sixteenth Symposium (International) on Combustion*, The Combustion Inst., Pittsburgh, PA, 1976, pp. 619–630.

[5]Khalil, E. E., and Whitelaw, J. H., "Aerodynamic and Thermodynamic Characteristics of Kerosene-Spray Flames," *Sixteenth Symposium (International) on Combustion*, The Combustion Inst., Pittsburgh, PA, 1976, pp. 569–576.

[6]Bachalo, W. D., and Houser, M. J., "Phase/Doppler Spray Analyzer for Simultaneous Measurements of Drop Size and Velocity Distributions," *Optical Engineering*, Vol. 23, No. 5, 1984, pp. 583–590.

[7]Mao, C.-P., Wang, G., and Chigier, N., "An Experimental Study of Air-Assist Atomizer Spray Flames," *Twenty-First Symposium (International) on Combustion*, The Combustion Inst., Pittsburgh, PA, 1986, pp. 665–673.

[8]McDonell, V. G., and Samuelsen, G. S., "Application of Two-Component Phase Doppler Interferometry to the Measurement of Particle Size, Mass Flux, and Velocities in Two-Phase Flows," *Twenty-Second Symposium (International) on Combustion*, The Combustion Inst., Pittsburgh, PA, 1988, pp. 1961–1971.

[9]Edwards, C. F., Rudoff, R. C., and Bachalo, W. D., "Measurement of Correlated Drop Size and Velocity Statistics, Size Distribution, and Volume Flux in a Steady Spray Flame," Fifth International Symposium on the Applications of Laser Techniques to Fluid Mechanics, Lisbon, Portugal, July 1990.

[10]Edwards, C. F., and Rudoff, R. C., "Structure of a Swirl-Stabilized Spray Flame by Imaging, Laser Doppler Velocimetry, and Phase Doppler Anemometry," *Twenty-Third Symposium (International) on Combustion*, The Combustion Inst., Pittsburgh, PA, 1990, pp. 1353–1359.

[11]Ghaffarpour, M., and Chehroudi, B., "Experiments on Spray Combustion in a Gas Turbine Model Combustor," *Combustion Science and Technology*, Vol. 92, Nos. 1–3, 1993, pp 173–200.

[12]McDonell, V. G., and Samuelsen, S., "Gas and Drop Behavior in Reacting and Non-Reacting Air-Blast Atomizer Sprays," *Journal of Propulsion*, Vol. 7, No. 5, 1991, pp. 684–691.

[13]Hassa, C., Deick, A., and Eickhoff, H., "Investigation of the Two-Phase Flow in a Research Combustor Under Reacting and Non-Reacting Conditions," *Fuels and Combustion Technology for Advanced Aircraft Engines, Propulsion and Energetics Panel 81st Symposium*, Fiuggi, Italy, 1993, pp. 41-1–41-12 (AGARD-CP-536).

[14]McDonell, V. G., Adachi, M., and Samuelsen, G. S., "Structure of Reacting and Non-Reacting Swirling Air-Assisted Sprays," *Combustion Science and Technology*, Vol. 82, Nos. 1–6, 1992, pp. 225–248.

[15]Presser, C., Gupta, A. K., and Semerjian, H. G., "Aerodynamic Characteristics of Swirling Spray Flames: Pressure-Jet Atomizer," *Combustion and Flame*, Vol. 92, Nos. 1–2, 1993, pp. 25–44.

[16]Zurlo, J. R., Presser, C., Gupta, A., and Semerjian, H. G., "Determination of Droplet Characteristics in Spray Flames Using Three Different Sizing Techniques," AIAA Paper 91-2200, June 1991.

[17]Shuen, J.-S., Solomon, A. S. P., and Faeth, G. M., "The Structure of Dilute Combusting Sprays," NASA CP 174838, Jan. 1985.